Depth-dependent phase change in Gd2O3 epitaxial layers under ion irradiation

N. Mejai, A. Debelle, L. Thome, G. Sattonnay, D. Gosset, Alexandre Boulle, R. Dargis, A. Clark

▶ **To cite this version:**

N. Mejai, A. Debelle, L. Thome, G. Sattonnay, D. Gosset, et al.. Depth-dependent phase change in Gd2O3 epitaxial layers under ion irradiation. Applied Physics Letters, 2015, 107 (13), pp.131903. 10.1063/1.4932089 . hal-02193703

HAL Id: hal-02193703
https://hal.science/hal-02193703

Submitted on 24 Jul 2019

HAL is a multi-disciplinary open access archive for the deposit and dissemination of scientific research documents, whether they are published or not. The documents may come from teaching and research institutions in France or abroad, or from public or private research centers.

L'archive ouverte pluridisciplinaire **HAL**, est destinée au dépôt et à la diffusion de documents scientifiques de niveau recherche, publiés ou non, émanant des établissements d'enseignement et de recherche français ou étrangers, des laboratoires publics ou privés.

Depth-dependent phase change in Gd_2O_3 epitaxial layers under ion irradiation

N. Mejai[1], A. Debelle[1*], L. Thomé[1], G. Sattonnay[1], D. Gosset[2], A. Boulle[3], R. Dargis[4], A. Clark[4]

1. Centre de Sciences Nucléaires et de Sciences de la Matière (CSNSM - UMR 8609),
Univ. Paris-Sud – CNRS/IN2P3, Bâtiment 108, 91405 Orsay Cedex, France
2. CEA-Saclay, DEN-DMN-SRMA-LA2M, Gif/Yvette, France
3. Science des Procédés Céramiques et de Traitements de Surface CNRS UMR 7315, Centre Européen de la Céramique, 12 rue Atlantis, 87068 Limoges, France
4. Translucent Inc., 952 Commercial St., Palo Alto, California 94303, USA

*Corresponding author: aurelien.debelle@u-psud.fr

Abstract

Epitaxial Gd_2O_3 thin layers with the cubic structure were irradiated with 4-MeV Au^{2+} ions in the 10^{13}-10^{15} cm^{-2} fluence range. X-ray diffraction indicates that ion irradiation induces a cubic to monoclinic phase change. Strikingly, although the energy-deposition profile of the Au^{2+} ions is constant over the layer thickness, this phase transformation is depth-dependent, as revealed by a combined X-ray diffraction and ion channeling analysis. In fact, the transition initiates very close to the surface and propagates inwards, which can be explained by an assisted migration process of irradiation-induced defects. This result is promising for developing a method to control the thickness of the rare-earth oxide crystalline phases.

Rare-earth oxides (REOs) of chemical formula RE_2O_3 (RE = La through Lu) exhibit different crystallographic structures (or phases) [1]. For instance, and of interest in the present study, gadolinium (Gd) oxide has a cubic, bixbyite C-form ($Ia\bar{3}$) at normal room temperature (RT) and ambient pressure, but the monoclinic B-form ($C2/m$) becomes stable at 1500 K at ambient pressure. Since the C-to-B phase transition is accompanied by volume contraction, the B-phase is stabilized at lower temperature with increasing pressure [1].

REO-based materials are becoming critical to a variety of high-technology products, including flat panel displays and batteries for hybrid vehicles (see e.g. [2] and references therein); due to their radiation-resistance property, they are also studied for nuclear energy applications [3-6] or, particularly Gd_2O_3 (GO), as solid-state neutron detectors [7]. As thin (epitaxial) layers grown on silicon, they represent, intrinsically or after doping, possible high-k (dielectric constant) gate dielectrics for modern metal-oxide-semiconductor devices [8]. They can also be buffers for growth of alternative semiconductors, the choice of which depends on the phase of the REO layer underneath [9]; regarding the REO phase, it has also been shown in GO that the monoclinic structure has a higher k value than its cubic counterpart [10]. In the case of these microelectronics applications, designing layers with control over composition, dopant concentration and crystallographic structure would be highly desirable for high-performance devices.

For this purpose, ion irradiation and/or implantation could be a promising route. Indeed, ion implantation is a process that allows tuning the dopant depth concentration, even above thermodynamic solubility [11]. Ion irradiation (i.e. with no purpose of incorporating foreign species) is used for creating defects in materials to modify their physical properties (as in, e.g., ZnO [12]). This technique can also lead to phase change at

different length scales, which includes crystalline-to-amorphous [13-14], crystalline-crystalline [14-16] or amorphous-to-crystalline phase transformations [17-18] for potential technological applications [19-20]. In the particular case of some REOs (e.g. Dy_2O_3 or Gd_2O_3), it has been shown, in textured thin films [6] and in polycrystalline pellets [4-5,21-22], that the cubic C-form can be transformed into the monoclinic B-form upon ion irradiation. However, no study has been undertaken so far in epitaxial, high-crystalline quality thin REO layers.

Crystalline REO (cREO^{TM}) layers deposited on silicon wafers have been developed for microelectronics applications by the Translucent Inc. Company. In this Letter, we present results on the behavior of one of these types of layers, namely cubic {111}-oriented Gd_2O_3 epitaxial layers, under ion irradiation. We show that in this designed material ion irradiation can stabilize the monoclinic structure of the REO at normal ambient conditions. More remarkably, it is observed a depth-dependence of the phase change, with the relative thickness of the two phases being dependent on the ion fluence.

The samples were grown by molecular beam epitaxy (MBE) on Si(111) wafers in a Veeco Gen20 MBE system using thermal evaporation of Gd in the presence of molecular oxygen. Details on the layer growth method and structural characteristics such as epitaxial relationship can be found in [23] and in the supplemental material [24]. As expected, the layer thickness was ~390 nm and the stoichiometric ratio was Gd/O = 2/3, as determined by Rutherford backscattering spectroscopy (RBS) analyses (see Fig.S2 of [24]). Samples where then subjected to 4-MeV Au^{2+} ion irradiation at RT in the $0.25x10^{14}$ to $50x10^{14}$ cm^{-2} fluence range. Irradiation details obtained using the dedicated SRIM code [25], such as energy-loss distributions (Fig.S3) and Au ion depth profile (Fig.S4), are provided in the supplemental material [24]. It is important to mention here that Au ions are essentially implanted in the Si

substrate, with only 0.1% at the GO-Si interface at the highest irradiation fluence ($50x10^{14}$ cm^{-2}); such a small impurity content should not affect the crystalline lattice in this material, as evidenced in other fluorite-type oxides [26-27]. Both pristine and irradiated layers were characterized by RBS in random and channeling (RBS/C) modes and by X-ray diffraction (XRD). For RBS experiments, a 1.4-MeV He^+ beam probe was used, and the detector was placed at a 165° angle. Owing to the experimental conditions, a depth resolution of about 10 nm was achieved (this value holds at the surface but slightly degrades deeper in the material due to energy straggling, see details in [24]). Both symmetric and asymmetric XRD measurements were performed; specifications of the set-ups can be found in [28] and [29], respectively. Symmetric measurements were conducted in high-resolution configuration using the $CuK_{\alpha 1}$ radiation selected by a 4xGe(220) monochromator, and a crystal analyzer in front of a point detector. Asymmetric measurements were performed in low incidence geometry using an INEL goniometer equipped with a Ge(111) monochromator to select the $CuK_{\alpha 1}$ radiation, and a fixed 120° 2θ-range curved position sensitive detector.

Simulation of the raw RBS spectra (these spectra are plotted in Fig.S2 of the supplemental material [24]) acquired in channeling geometry was realized using a dedicated code (McChasy code [30]) which assumes that a disordered crystalline material contains a fraction of defects, hereby called f_D, as a form of randomly displaced atoms. Fitting of the spectra thus allowed obtaining the f_D depth distributions displayed in Fig.1. It must be noted that in Fig.1 is also shown the profile of a layer obtained in random geometry (dashed line) for a pristine sample: disorder saturates in this case at 100% over the entire layer thickness because channeling is impossible in this configuration. Nonetheless, the pristine layer is of very good crystalline quality, as indicated by the very low value of f_D (~1%) in the profile recorded in channeling geometry (black line in Fig.1). It must be noticed that f_D is higher at

the GO-Si interface where a slight increase in the disorder (a few percent) is detected over a ~30-nm thickness. Previous observations of these same layers by high-resolution transmission electron microscopy showed that the interface is clean and abrupt [23]. However, this result from ion channeling indicates that the interface is not perfect but probably contains a low dislocation density, as observed in other epitaxially-grown films [31].

After irradiation, three zones can be distinguished as a function of depth. Starting from the surface, in zone I, the disorder progressively increases to reach the maximum level (100%) at 35 x10^{14} cm^{-2}. Under this uppermost region, zone II is almost defect-free even at the highest ion fluence. Zone III is located at the backside of zone II and extends up to the GO-Si interface. Although disorder in this third zone also increases with fluence as in zone I, it does not reach full disorder but only a maximum of 45% (except in the initially perturbed 30-nm width interface region with Si where a 80% disorder is measured). Note that the Si substrate is amorphized over a few hundreds of nanometers after the first irradiation fluences (not shown in Fig.1). The thickness of the three zones depends on the ion fluence, and interfaces between them are not sharp. For instance, zone I, which is ~100 nm thick at 35x10^{14} cm^{-2}, has an interface that extends over ~30 nm; at 50x10^{14} cm^{-2}, it has a ~170-nm thickness. Necessarily, zone II shrinks between these two fluences, from ~170 nm to ~40 nm. Zone III corresponds to the remaining backside layer.

The 100% disorder level determined in zone I by RBS/C in layers irradiated at high fluence can be due to an amorphization of the layer, to a crystalline-to-crystalline phase change and/or to the formation of a polycrystalline structure. Low-incidence XRD measurements were performed on the layer irradiated at 50x10^{14} cm^{-2} (Fig.2) to determine the origin of this high disorder level. Two different incidence angles, 1° and 4°, were chosen.

The corresponding X-ray penetration depths were calculated using the method described in [32-33]. Considering an attenuation factor of (1-1/e), these depths were calculated to be ~65 nm and ~270 nm at 1° and 4°, respectively. The 1° angle was selected to probe the near-surface layer, while the 4° angle was chosen to investigate the entire thickness altered by ion irradiation (i.e. ~250 nm, see Fig.1). Moreover, in order to detect any texture effect, the scan at 4° was performed with and without the use of the sample spinner.

For the pristine layer, no peak is detected in the large 25°-65° 2θ-range, which is fully consistent with the epitaxial nature of the layers for which no reflection is accessible in this geometry. On the contrary, for the irradiated sample ($50x10^{14}$ cm^{-2}), several peaks are detected in the scan acquired at 4° using the sample spinner (red curve in Fig.2), meaning that the layer did not undergo amorphization. Besides, all the peaks can be ascribed to the monoclinic structure, which indicates that RBS/C results may be interpreted in terms of a C-to-B phase change. No major reflection corresponding to the cubic structure can be observed (note in Fig.2 the absence of the $(222)_c$, $(400)_c$ and $(440)_c$ peaks that do not overlap with peaks from the monoclinic form); this finding indicates that there is no polycrystalline cubic phase in the layer. In the scan recorded at 1°, numerous peaks of the B-form are already visible, which indicates that the monoclinic phase is present in the first tens of nanometers, and thus that the phase change took place from the surface.

Symmetric (high-angle) XRD measurements of the (444) reflection of the {111}-oriented GO layers are presented in Fig.3 (note that a slight offset was applied in order to avoid the unnecessary (222) reflection of the thick undamaged part of the Si substrate). It is observed that whatever the ion fluence, the cubic phase is still present because the (444) reflection of the GO C-form remains visible. Since the B-form is present in the surface layer, as revealed by the results of asymmetric XRD, the remaining epitaxial C-form layer must be

located beneath (although the presence in the surface layer of small regions of cubic {111}-oriented GO cannot be completely ruled out). Therefore, the whole XRD measurements demonstrate the depth dependence of the phase transition.

Several reflections of the monoclinic structure are recorded in low-incidence XRD, meaning that there is no unique orientation relationship between the B-phase at the top of the layer and the C-phase beneath since this latter remains single-crystal-like, i.e with a unique crystallographic orientation. This result is different to what was observed in irradiated Dy_2O_3, where a $\left[1\bar{1}0\right]_c // \left[1\bar{3}2\right]_m, \{222\}_c // (40\bar{2})_m$ orientation relationship was noted (c denotes cubic and m stands for monoclinic), but the samples were polycrystalline pellets [34]; more work is needed here to determine whether there is topotaxic relationship(s) between the two phases. Yet, a moderate texture is evidenced by the difference in relative peak intensities in XRD patterns recorded with and without using the sample spinner (see the two scans at 4° in Fig.2.). XRD peaks recorded at 4° (red curve in Fig.2) are quite broad and are mainly Gaussian. Considering that the peak broadening is only due to finite size effect, and taking into account the non-negligible geometric contribution associated to low-incidence XRD measurements [35], one can use the well-known Scherrer equation that links peak integral breadth and coherent diffraction domain size to estimate this latter [36]. An average value of ~35 $\pm$ 5 nm was found. This value is underestimated since microstrains, arising from extended defects (see discussion below and [6]), also contribute to peak broadening. Nevertheless, such a small dimension strongly suggests that the phase transition proceeds from heterogeneous nucleation of B-form domains. This assumption was also speculated in [4], and likewise it was shown in irradiated textured Y_2O_3 thin films that the C-to-B transition is preceded by the formation of a high density of dislocations that leads to a fragmentation of the crystallites into nanograins [6]. To finish,

the positions of the XRD peaks correspond to those for an unstrained monoclinic structure. Both the decrease in the molar volume during the C-to-B transition [1], and the likely formation of extended defects prior to phase transition [6] could explain that the strain build-up is prevented in the B-form regions.

The occurrence of two different phases as a function of the thickness was observed in epitaxially grown GO on Ge(001) substrates: GO was found to start growing cubic but rapidly, in the first ten nanometers, the monoclinic phase settled [37]. This phase transition was ascribed to strain fields between the crystal structures. It has been clearly demonstrated in numerous cases that low-energy ion irradiation induces a tensile strain that develops only along the surface normal direction [38,39], this strain being the consequence of the formation of crystalline defects. In Fig.3, it is observed that the normal strain, in the C-form layer, remains low (0.3% at max.) and that it starts to be relieved at very low fluence ($1.25x10^{14}$ cm^{-2}). The strain relaxation, which occurs concomitantly with the amorphization of the Si substrate at the GO-Si interface, could be explained by a loss of firm registry (coherence) between the GO and the Si lattices, and/or by a slight substrate bending due to an amorphization-induced swelling. Anyway, the strain, which does not exceed 0.3% and which is rapidly relieved, cannot be the main origin of the observed phase transition.

Another explanation for the C-to-B phase change is related to defect production and accumulation due to energy deposition upon ion irradiation, as previously shown in irradiated REOs [4-6] but also in other fluorite-type-structured materials [14-16]. Actually, defect formation during irradiation leads to an increase in the system energy, and phase transition is a way for the material to decrease the energy stored upon irradiation. Using the SRIM code [25], we calculated the two contributions of the Au ions slowing down process, namely the electronic (S_e) and nuclear (S_n) energy-loss depth distributions (see details of the

calculations and corresponding profiles – Fig.S3 - in the supplemental material [24]). Both contributions are nearly constant over the entire GO layer thickness, with a same level of ~4.5 keV/nm, which is enough to induce a significant number of displaced atoms. However, the energy-deposition depth distribution seems to be incompatible with the observed phase-change depth profile, because the latter is depth-dependent while the former is not. In particular, the C-to-B transition initiates in zone I, *i.e.* close to the surface, and it does not take place simultaneously over the entire layer thickness whereas both S_e and S_n are constant. This is an atypical phase change because such a process usually occurs in the region of high S_n [40-42], or in the region where S_e exceeds a threshold value [43].

In order to account for the depth dependence, in addition to defect creation by ion irradiation, defect migration and accumulation at the layer surface should be invoked. There could be several driving forces for such a defect migration to take place. First, the irradiation-induced normal tensile strain that develops in the first irradiation stage, and/or the stress induced by the curvature of the Si substrate after its amorphization close to the GO/Si interface could lead to anisotropic defect mobility (see e.g. [44] and references therein), with an enhanced migration along the surface normal. Second, a chemical gradient due to intermixing at the GO-Si interface on the one hand and stoichiometric GO at the layer surface on the other hand, could also lead to defect migration along the surface normal [45]. Third, defects are most likely charged in this iono-covalent material, and electric fields could also play a role in their migration, particularly owing to the non-negligible electronic energy-loss (see S_e in Fig.S3.) that induces localized excitations or ionizations [46,47]. A combination of these driving forces, which could act simultaneously or at different stages of the irradiation process, could also be considered. A detailed investigation is currently under way to get a better understanding of this phenomenon; for instance, a change in the ion

stopping range and in the energy regime (S_e/S_n ratio) is investigated. This assumption of defect migration to the surface would explain why a defect-depleted region, which remains cubic and oriented, is sandwiched between the transformed surface layer and the interface region with Si that becomes defective (presumably due to intrinsic defects that may act as traps for irradiation defects).

In summary, Gd_2O_3 epitaxially grown layers on Si substrates experience a cubic to monoclinic phase change upon ion irradiation at normal ambient conditions. In these layers, the phase change initiates at the surface and propagates inwards, progressively consuming the cubic region. This process offers a promising route to control the thickness of the crystalline phases in REO layers. It is worth mentioning that this phase change could also be obtained by ion implantation (and not only irradiation) where both doping and structural transformation would be jointly carried out. Finally, in an attempt to prepare multilayered materials for microelectronics applications, it might be desirable to try to reduce the defect density and recrystallize the Si at the GO-Si interface, while preserving the different crystallographic structures. For this purpose, ion irradiation/implantation above room temperature and/or subsequent thermal annealing could be envisaged.

ACKNOWLEDGEMENTS

CSNSM members would like to thank the SEMIRAMIS staff, and particularly C. Bachelet, J. Bourçois and S. Picard for the samples irradiation and for their assistance during RBS/C measurements. HRXRD measurements on the Panalytical diffractometer have been performed at the nanocenter CTU-IEF-Minerve that is partially funded by the “Conseil Général de l’Essonne”. N. Mejai is grateful to “Région Ile-de-France” and “DIM-OxyMORE” for funding her PhD thesis; she is also indebted to the CSNSM management staff for cautiously taking care of her health.

REFERENCES

[1] M. Zinkevich, Prog. Mater. Sci. 52 (2007) 597.

[2] Scientific Investigations Report of U.S. Geological Survey, reference sir2011-5094, 2011. http://pubs.usgs.gov/sir/2011/5094/pdf/sir2011-5094.pdf

[3] R.C. Ewing, W. J. Weber, J. Mater. Res. 10 (1995) 243.

[4] M. Tang, P. Lu, J. A. Valdez, K. E. Sickafus, J. Appl. Phys. 99 (2006) 063514.

[5] M. Tang, J. A. Valdez, K. E. Sickafus, P. Lu, Appl. Phys. Lett. 90 (2007) 151907.

[6] R. J. Gaboriaud, F. Paumier, M. Jublot, B. Lacroix, Nucl. Instr. Methods. B 311 (2013) 86.

[7] A. N. Caruso, J. Phys.: Condens. Matter 22 (2010) 443201.

[8] P. Shekhter, A.R. Chaudhuri, A. Laha, S. Yehezkel, A. Shriki, H.J. Osten, M. Eizenberg, App. Phys. Lett. 105 (2014) 262901.

[9] R. Dargis, A. Clark, F. E. Arkun, T. Grinys, R. Tomasiunas, A. O'Hara, A. A. Demkov, J. Vac. Sci. Technol. A 32 (2014) 041506.

[10] D. A. Grave, Z. R. Hughes, J. A. Robinson, Th. P. Medill, M. J. Hollander, A. L. Stump, M. Labella, X. Weng, D. E. Wolfe, Surf. Coat. Technol. 206 (2012) 3094.

[11] L. A. Larson, J. M. Williams, M. I. Current, Rev. Accl. Sci. Tech. 04 (2011) 11.

[12] B Panigrahy, M. Aslam, D. Bahadur, Appl. Phys. Lett. 98 (2011) 183109.

[13] S.U. Campisano, S. Coffa, V. Raineri, F. Priolo, E. Rimini, Nucl. Instr. Meth. B 80 (1993) 514.

[14] G. Sattonnay, S. Moll, L. Thomé, C. Decorse, C. Legros, P. Simon, J. Jagielski, I. Jozwik, I. Monnet, J. Appl. Phys. 108 (2010) 103512.

[15] K. E. Sickafus, R. W. Grimes, J. A. Valdez, A. Cleave, M. Tang, M. Ishimaru, S. M. Corish, Ch. R. Stanek, B. P. Uberuaga, Nature Materials 6 (2007) 217.

[16] M. Lang, F. Zhang, J. Zhang, J. Wang, B. Schuster, Ch. Trautmann, R. Neumann, U. Becker, R. C. Ewing, Nature Materials 8 (2009) 793.

[17] I. Ivan, S. Kokenyesi, A. Csik, Chalcogenide Letters 4 (2007) 115.

[18] A. Debelle, M. Backman, L. Thomé, W. J. Weber, M. Toulemonde, S. Mylonas, A. Boulle, O. H. Pakarinen, N. Juslin, F. Djurabekova, K. Nordlund, F. Garrido, and D. Chaussende, Phys. Rev. B 86 (2012) 100102 (R).

[19] R. Spohr, "Ion Tracks and Microtechnology: Principles and Applications", Ed. K. Bethge, Vieweg 1990, Germany.

[20] D. Fink, L. T. Chadderton, Brazilian Journal of Physics 35 (2005) 735.

[21] M. Lang, F. Zhang, J. Zhang, C. L. Tracy, A. B. Cusick, J. VonEhr, Z. Chen, Ch. Trautmann, R. C. Ewing, Nucl. Instr. Meth. B 326 (2014) 121.

[22] D. R. Rittman, C. L. Tracy, A. B. Cusick, M. J. Abere, B. Torralva, R. C. Ewing, S. M. Yalisove, Appl. Phys. Lett. 106 (2015) 171914.

[23] R. Dargis, D. Williams, R. Smith, E. Arkun, R. Roucka, A. Clark, M. Lebby, ECS J. Solid State Sc. And Technol. 1 (2012) 24.

[24] Supplemental material at [URL will be inserted by AIP]

[25] J.F. Ziegler, J. P. Biersack, U. Littmark, The Stopping and Range of Ions in Solids, Pergamon, New York, 1985. Available at: www.srim.org.

[26] S. Moll, L. Thomé, G. Sattonnay, A. Debelle, F. Garrido, L. Vincent, J. Jagielski, J. Appl. Phys. 106, (2009) 073509.

[27] T. Yang, C. A. Taylor, Sh. Kong, Ch. Wang, Y. Zhang, X. Huang, J. Xue, Sha Yana, Y. Wang, J. Nucl. Mater. 443 (2013) 40.

[28] A. Debelle, L. Qasim, P. Rosza, S. Moll, A. Boulle, L. Thomé, Nucl. Instr. Meth. B277 (2011) 14.

[29] D. Gosset, M. Le Saux, D. Simeone, D. Gilbon, J. Nucl. Mater. 429 (2012) 19.

[30] L. Nowicki, A. Turos, R. Ratajczak, A. Stonert, F. Garrido, Nucl. Instr. Meth. B240 (2005) 277.

[31] B. Holländer, S. Mantl, M. Mayer, C. Kirchner, A. Pelzmann, M. Kamp, S. Christiansen, M. Albrecht, H. P. Strunk, Nucl. Instr. Meth. B 136-138 (1998) 1248.

[32] D. Simeone, G. Baldinozzi, D. Gosset, S. Le Caer, J.-F. Bérard, Th. Sol. Films 530 (2013) 9.

[33] G. Renaud, R. Lazzari, F. Leroy, Surf. Sci. Reports 64 (2009) 255.

[34] M. Tang, P. Lu, J. A. Valdez, K. E. Sickafus, Phil. Mag. 86 (2006) 1597.

[35] A. Boulle, O. Masson, R. Guinebretière, A. Lecomte, A. Dauger, J. Appl. Cryst. 35 (2002) 606.

[36] “Powder Diffraction: Theory and Practice”, chap. 13, by R. E. Dinnebier, S. J. L. Billinge, A. Le Bail, I. Madsen, L. M. D. Cranswick, RCS Publishing (2008).

[37] A. Molle, C. Wiemer, Md. N. K. Bhuiyan, G. Tallarida, M. Fanciulli, Appl. Phys. Lett. 90 (2007) 193511.

[38] A. Debelle, A. Declémy, Nucl. Instr. Meth. B 268 (2010) 1460.

[39] A. Boulle, A. Debelle, J. Appl. Cryst. 43 (2010) 1046.

[40] S. Moll, G. Sattonnay, L. Thomé, J. Jagielski, C. Decorse, P. Simon, I. Monnet, and W. J. Weber, Phys. Rev. B. 84, 064115 (2011).

[41] Y. Zhang, J. Jagielski, I.-T. Bae, X. Xiang, L. Thomé, G. Balakrishnan, D. M. Paul, W. J.Weber, Nucl. Instr. Meth. B 268 (2010) 3009.

[42] Y. Zhang, C. M. Wang, M. H. Engelhard, W. J. Weber, J. Appl. Phys. 100 (2006) 113533.

[43] M. Lang, R. Devanathan, M. Toulemonde, Ch. Trautmann, Current Opinion in Solid State and Materials Science 19 (2015) 39.

[44] P. Castrillo, R. Pinacho, M. Jaraiz, J. E. Rubio, J. Singer, Mater. Science and Eng. B 154 (2008) 260.

[45] “Diffusion in Oxides” by M. Martin in “Diffusion in Condensed Matter”, Eds. P. Heitjans and J. Kärger, Springer-Verlag Berlin Heidelberg (2005).

[46] S.J. Zinkle, V.A. Skuratov, D.T. Hoelzer, Nucl. Instr. Meth. B 191 (2002) 758.

[47] W. J. Weber, D. M. Duffy, L. Thomé, Y. Zhang, Current Opinion in Solid State and Materials Science 19 (2015) 1.

FIGURE CAPTIONS

Fig.1: Disorder depth profiles derived from simulations, with the McChasy code [30], of RBS/C data obtained for pristine and 4-MeV Au^{2+} ion-irradiated GO layers. Fluences are expressed in 10^{14} cm^{-2}. The dashed line corresponds to a pristine layer as seen in random geometry. The depth dependence phase-change is materialized by the three zones observed at the highest irradiation fluence: zone I, where the monoclinic phase is present (f_D=100%), zones II which is weakly disordered (f_D~10%) and zone III being mainly the interfacial region between the GO layer and the Si substrate.

Fig.2: Low-incidence XRD patterns recorded at two different angles (1° and 4°) on a 4-MeV Au^{2+} ion irradiated ($50x10^{14}$ cm^{-2}) GO layer. Curves are shifted vertically for visualization purposes. The curve corresponding to a pristine layer (and recorded at 4°) is also displayed as a black dashed line. Patterns marked with a star (*) were acquired with the spinning mode. Vertical thin solid lines at the bottom of the graph indicate the position of the reflections for the unstrained monoclinic structure, while grey arrows indicate the positions of a few major reflections for the cubic form (c denotes cubic).

Fig.3: High-resolution XRD symmetric scans recorded in the vicinity of the (444) reflection of pristine and 4-MeV Au^{2+} irradiated GO thin layers at indicated fluences. Curves are shifted vertically for visualization purposes. The vertical dashed line indicate the peak position for a pristine layer (*i.e.* the zero-strain level), and arrows show the variation of the normal strain with ion fluence.

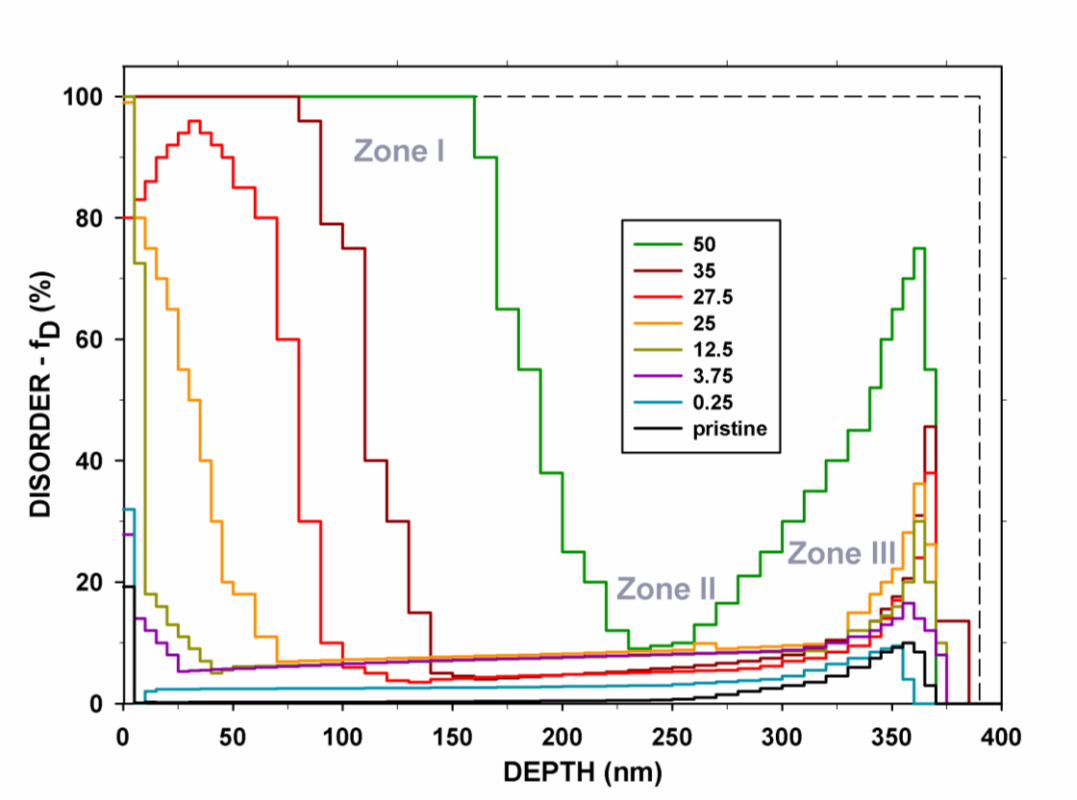
Zone I
Zone II
Zone III
50
35
27.5
25
12.5
3.75
0.25
pristine
DISORDER - f_D (%)
DEPTH (nm)
0
20
40
60
80
100
0
50
100
150
200
250
300
350
400

Figure 1

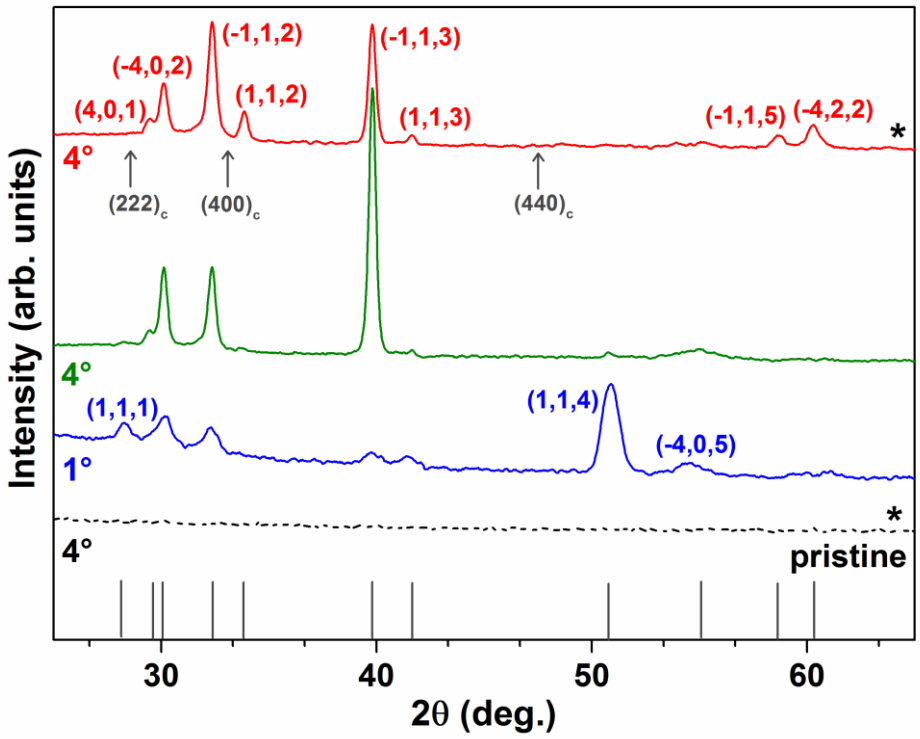
Intensity (arb. units)
(4,0,1)
(-4,0,2)
(-1,1,2)
(1,1,2)
(-1,1,3)
(1,1,3)
(-1,1,5)
(-4,2,2)
*
4°
(222)c
(400)c
(440)c
4°
(1,1,1)
(1,1,4)
(-4,0,5)
1°
*
4°
pristine
30
40
50
60
2θ (deg.)

FIGURE 2

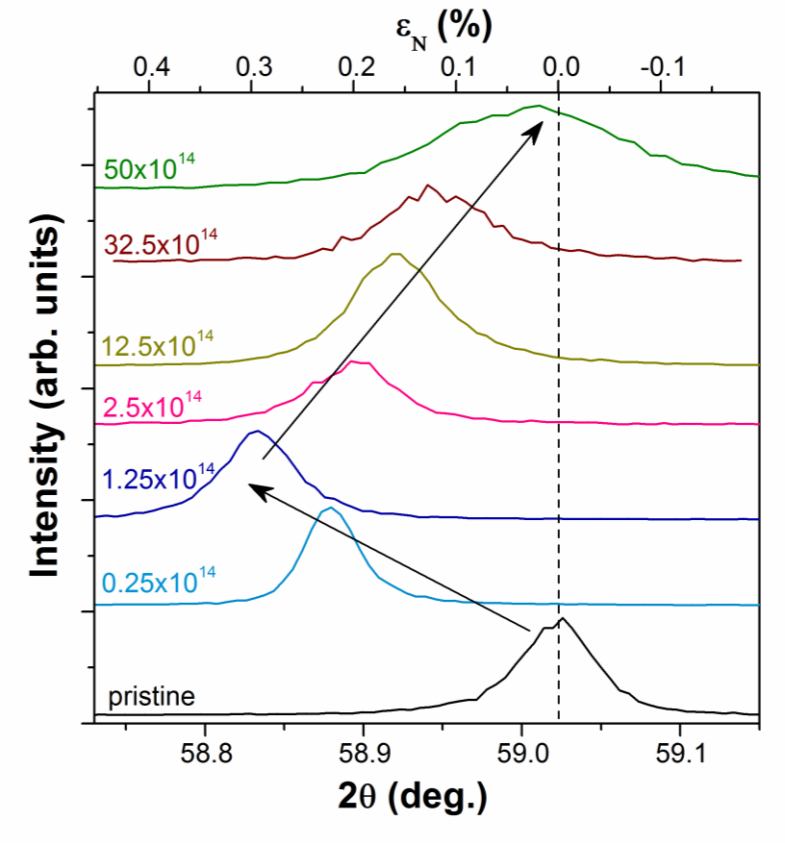
ε_N (%)
0.4
0.3
0.2
0.1
0.0
-0.1
50x10^14
32.5x10^14
12.5x10^14
2.5x10^14
1.25x10^14
0.25x10^14
pristine
Intensity (arb. units)
58.8
58.9
59.0
59.1
2θ (deg.)

FIGURE 3